Asia-Pacific Journal of Science and Technology: Volume: 29. Issue: 02. Article ID.: APST-29-02-06. Research Article

APST

Asia-Pacific Journal of Science and Technology

https://www.tci-thaijo.org/index.php/APST/index

Published by the Research and Graduate Studies Division,
Khon Kaen University, Thailand

N501Y mutation in SARS-CoV-2 spike RBD protein enhances its binding to ACE2 receptor

Napat Kongtaworn[1], Nitchakan Darai[1], Panupong Mahalapbutr[2], Supot Hannongbua[3], Peter Wolschann[4] and Thanyada Rungrotmongkol[1,5,*]

[1] Program in Bioinformatics and Computational Biology, Graduate School, Chulalongkorn University, Bangkok, Thailand
[2] Department of Biochemistry, Faculty of Medicine, Khon Kaen University, Khon Kaen, Thailand
[3] Center of Excellence in Computational Chemistry (CECC), Department of Chemistry, Faculty of Science, Chulalongkorn University, Bangkok, Thailand
[4] Department of Theoretical Chemistry, University of Vienna, Vienna, Austria
[5] Center of Excellence in Biocatalyst and Sustainable Biotechnology, Department of Biochemistry, Faculty of Science, Chulalongkorn University, Bangkok, Thailand
[*]Corresponding author: t.rungrotmongkol@gmail.com

Received 15 October 2022
Revised 24 February 2023
Accepted 14 March 2023

Abstract

Studies have indicated that the N501Y mutation in the spike protein of SARS-CoV-2 enhances the binding efficiency between its receptor-binding domain (RBD) and the human angiotensin-converting enzyme 2 (ACE2) receptor, decreasing vaccine effectiveness and increasing the potential for viral infection. In this work, the structures of the wild-type RBD and N501Y-RBD in complex with the ACE2 receptor were generated to evaluate the effect of the N501Y mutation on their binding efficiency using molecular dynamics simulations, free energy calculations based on the MM/GB(PB)SA and SIE methods, and residue interaction network analysis. The results revealed that the N501Y-RBD/ACE2 complex displays higher compactness than the wild-type RBD/ACE2 structure via strong H-bonding, π–π, and van der Waals interactions. Moreover, the number of hot-spot residues in N501Y-RBD/ACE2 was higher than that of the wild-type RBD/ACE2 system. Structural and energetic insights gained from the study could be utilised for the design of novel drugs and vaccines against newly emerging coronavirus strains.

Keywords: SARS-CoV-2, S protein RBD–ACE2 binding, N501Y mutation, MD simulation, Residue interaction network analysis

1. Introduction

The outbreak of the severe acute respiratory syndrome coronavirus 2 (SARS-CoV-2) in 2019 has led to a global pandemic and over 613 million and 6.5 million confirmed cases and deaths, respectively, as reported by the World Health Organisation (WHO) in September 2022 [1]. Clinical symptoms of SARS-CoV-2 infection include a sore throat, dry cough, fever, and acute respiratory distress syndrome [2]. Regarding its structure, SARS-CoV-2 comprises a positive-sense, single-stranded RNA (+ssRNA) genome 30 kb in length along with an envelope, a membrane, an inner nucleocapsid, and spike (S) proteins [3, 4].

The S protein forms a major component of the surface of SARS-CoV-2, responding to human cell attachment and triggering membrane fusion [5]; as shown in Figure 1A, it consists of two subunits, namely S1 and S2 [6]. S1 contains a receptor-binding domain (RBD) that interacts with an angiotensin-converting enzyme 2 (ACE2) receptor found on the membranes of human lung cells [7, 8], while S2 allows for the fusion of viral and cellular membranes, resulting in the entry of SARS-CoV-2 into host cells [5]. Studies have revealed that N501, one of the

amino acids involved in the binding between ACE2 and the RBD, can mutate; such mutated virus strains have spread in the European Union (EU), South Africa, and Brazil [9-11].

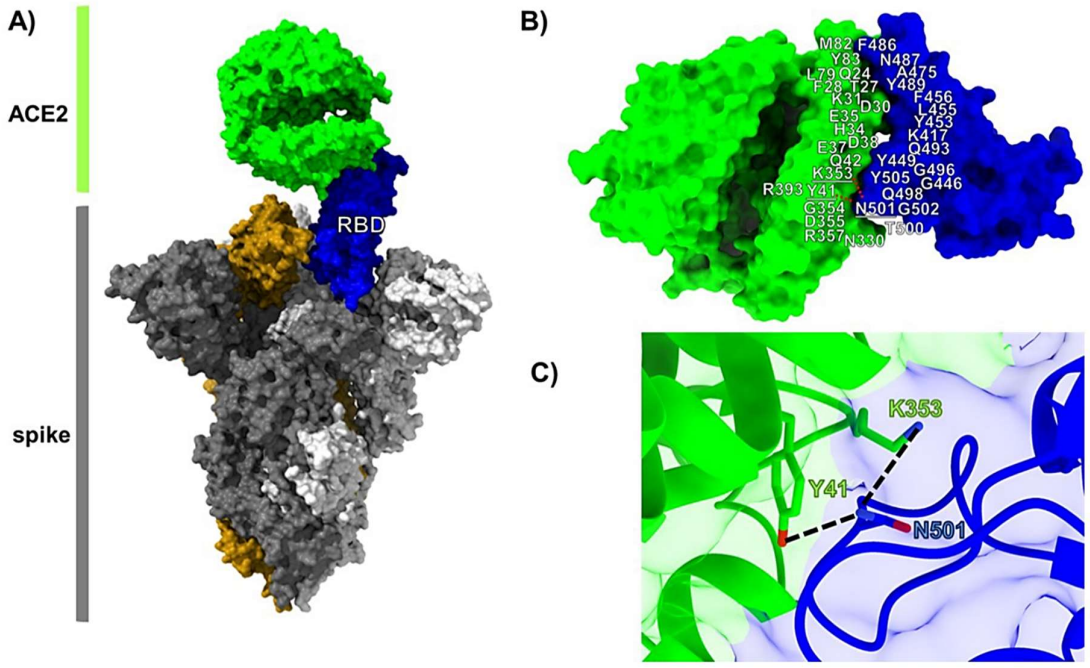

Figure 1 Crystal structure of the SARS-CoV-2 spike protein (PDB ID 7A94). The binding of the open form of the RBD (blue) to ACE2 (green) is presented, while the closed form of the RBD and S2 are represented in grey and dark grey, respectively. (A) represents the S protein binding to ACE2, (B) shows the complex formed between the RBD and ACE2 and amino acids within the interface area, and (C) depicts the binding interaction between N501 in the RBD and Y41 and K353 in ACE2 at the RBD–ACE2 interface.

The N501Y mutation of the SARS-CoV-2 S protein, located in the RBD binding site, has rapidly spread in England, Brazil, and South Africa [9-11]; according to the Global Initiative on Sharing Avian Influenza Data (GISAID), the N501Y mutations in England, South Africa, and Brazil are classified as 20I (20I/501Y.V1, Alpha), 20H (20H/501Y.V2, Beta), and 20J (20J/501Y.V3, Gamma), respectively. The cryo-EM structure of the SARS-CoV-2 spike RBD of the Alpha variant bound to the ACE2 receptor has been characterised [12]. Due to the N501Y mutation found in this variant, the mutated Y501 residue could interact with the Y41 and K353 residues of ACE2, resulting in increased binding affinity within the RBD/ACE2 complex [13]. Additionally, enhanced network interaction with ACE2 has been identified in the Alpha variant [14]. This study performs molecular dynamics (MD) simulations and free energy calculations – based on the molecular mechanics/generalised Born surface area (MM/GBSA), molecular mechanics/Poisson–Boltzmann surface area (MM/PBSA) [15], and solvated interaction energy (SIE) methods [16] – to compare the molecular-level interactions and susceptibility of the protein–protein complex in the N501Y mutation and wild-type (WT) systems. We aim to gain insights from the structural and binding results to help explain the binding patterns between the N501Y RBD SARS-CoV-2 species and the ACE2 receptor.

2. Materials and methods

2.1 Preparation of RBD structure

In the present work, the WT-RBD/ACE2 and N501Y-RBD/ACE2 complexes were investigated computationally. The initial structure for the WT-RBD/ACE2 complex (PDB ID 6M0J [17]) was retrieved from the RSCB Protein Data Bank, and the mutated N501Y residue in the RBD was generated from the WT crystal structure using AMBER's LEaP program [18], where the amino acid in the RBD at residue N501 was changed to Y501. Subsequently, the protonation states of ionisable amino acids of both complexes were checked at pH 7.0 using the PROPKA 3.0 web server [19]. The AMBER ff14SB force field [20] was applied for all proteins. In addition, the total charges of both systems were neutralised using sodium ions and the LEaP module. Moreover, the TIP3P

water model [21] was employed to solvate each protein complex, with a distance of 10 Å between the protein–protein complex and the edge of the octahedral periodic water box. The water molecules and hydrogen atoms were minimised to remove any bad contacts using the steepest descent (1000 steps) and conjugate gradient (2500 steps) methods, respectively. Finally, all the atoms were minimised using similar techniques.

2.2 MD simulations of N501Y- and WT-RBD/ACE2 systems

Both systems were simulated using periodic boundary conditions in the isothermal−isobaric (NPT) ensemble, as explained previously [22], and the SHAKE algorithm was used to constrain the covalent bonds involved with hydrogen atoms [23]. The charge-charge and non-bonded interactions within a 10 Å cutoff distance were computed using the particle mesh Ewald summation method [24]. A time step of 2 fs was applied, and in the relaxation step, the temperature and pressure were controlled using a Langevin thermostat with a collision frequency of 2 ps^{-1} and a Berendsen barostat with a pressure relaxation time of 1 ps. All protein atoms were then restrained using a harmonic constraint of 50.0 kcal/mol $Å^2$ while the systems were heated for 100 ps from 100 to 310 K. After heating, the complexes were equilibrated at 310 K with the same harmonic constraint for 1 ns. The systems were simulated for 100 ns under the NPT ensemble at the same temperature and pressure in the equilibration step, and coordinates were saved every 10 ps in the MD trajectories.

The trajectories were analysed using the CPPTRAJ module [25] in the AMBER16 program. The system stability was evaluated by measuring the root-mean-square deviation (RMSD) and the radius of gyration (Rg). In addition, the binding affinity between the RBD and ACE2 was investigated with binding free energy calculations using the MM/GBSA and MM/PBSA methods ($\Delta G_{\text{bind}}^{\text{MM/GBSA}}$ and $\Delta G_{\text{bind}}^{\text{MM/PBSA}}$), neglecting entropy contributions, and the SIE method. Regarding the percentage occupation of hydrogen bonds (%H-bonds), the distance and angle between H-bond donors and acceptors were set to ≤ 3.5 Å and ≥ 120°, respectively, to evaluate the intermolecular interactions between the RBD and ACE2. Furthermore, the residue contribution in the protein–protein binding was investigated using the per-residue decomposition free energy ($\Delta G_{\text{bind}}^{\text{residue}}$), computed by the MM/GBSA method. Moreover, the effect of the N501Y mutation was analysed by calculating the solvent-accessible surface area (SASA), the number of contact atoms (#contacts), and the protein–protein interaction between residue N/Y501 and ACE2. The residue interaction network was studied using the Residue Interaction Network Generator (RING 3.0) program [26]. A total of 100 snapshots from the last 30 ns of the MD trajectories was used to identify non-bonding interactions between residue N/Y501 and the ACE2 receptor. In this work, we used a program default to calculate the distances between each node, that is, with H-bonds ≤ 3.5 Å, ionic bonds ≤ 4 Å, π– cation interactions ≤ 5 Å, van der Waals (vdW) interactions ≤ 0.5 Å, π–π stacking ≤ 6.5 Å, and disulfide bonds ≤ 2.5 Å. Only > 40% occupation of intermolecular interactions was selected to form the edges using Cytoscape [27].

3. Results and discussion

3.1 Validation of the mutated RBD structure

The WT- and N501Y-RBD structures were validated using Ramachandran plots [28] (Figure 2) of the torsional angles – phi (φ) and psi (ψ) [29]. The highly preferred observations are 96.71% and 97.35% for the WT and N501Y systems, respectively, while the preferred observations are 1.31% for both systems. The questionable observations are 1.97% and 1.32% for the WT and N501Y systems, respectively. Notably, the 501 position in both systems was detected in a highly preferred region, in line with the stable secondary structure obtained within the simulation time (Figure 3). Although the cryo-electron microscopy (cryo-EM) structure of N501Y-RBD/ACE2 suggests a slightly altered conformation of the N501Y-RBD residues around the Y501 residue, the conformation in the secondary structure of the RBD is similar to that of WT-RBD/ACE2. Altogether, these results suggest that the mutated structure is acceptable.

3.2 Stability of WT- and N501Y-RBD/ACE2 systems

RMSD calculations were used to evaluate the WT- and N501Y-RBD/ACE2 system stability, as presented in Figure 4 (top). The RMSD values of the complex and ACE2 in the N501Y-RBD/ACE2 system increased significantly within the first 30 ns compared to the RMSD results in the WT-RBD/ACE2 system, indicating that the ACE2 conformation changed to enhance the fluctuations of the system due to the mutation of residue N501. In addition, the Rg results support the altering of the ACE2 conformation in the N501Y-RBD/ACE2 system, as shown in Figure 4 (bottom), indicating that the N501Y mutation can increase the compactness between N501Y-RBD and ACE2. The last 30 ns of the MD trajectories were employed for further structural and energetic analysis.

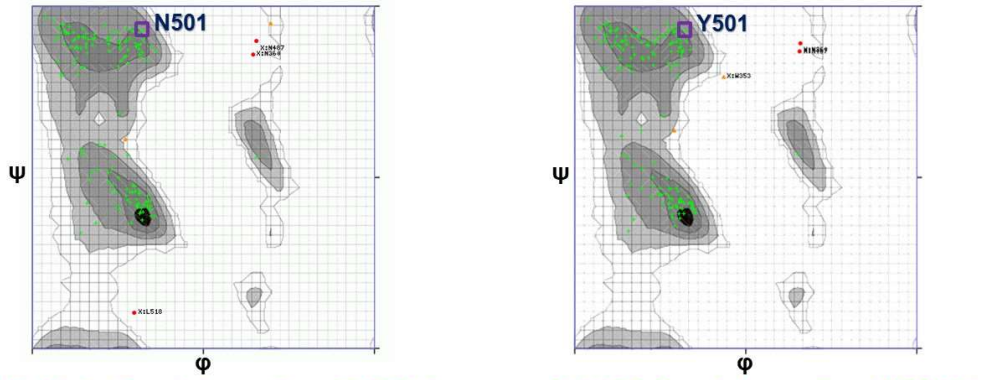

System	Residue	φ	ψ	ZONE
WT	N501	-63.69	154.42	Highly Preferred
N501Y	Y501	-62.64	154.34	Highly Preferred

Figure 2 Ramachandran plots for last 10 ns of simulation. The plot was generated from Ramachandran Plot Server (https://www.umassmed.edu/zlab/).

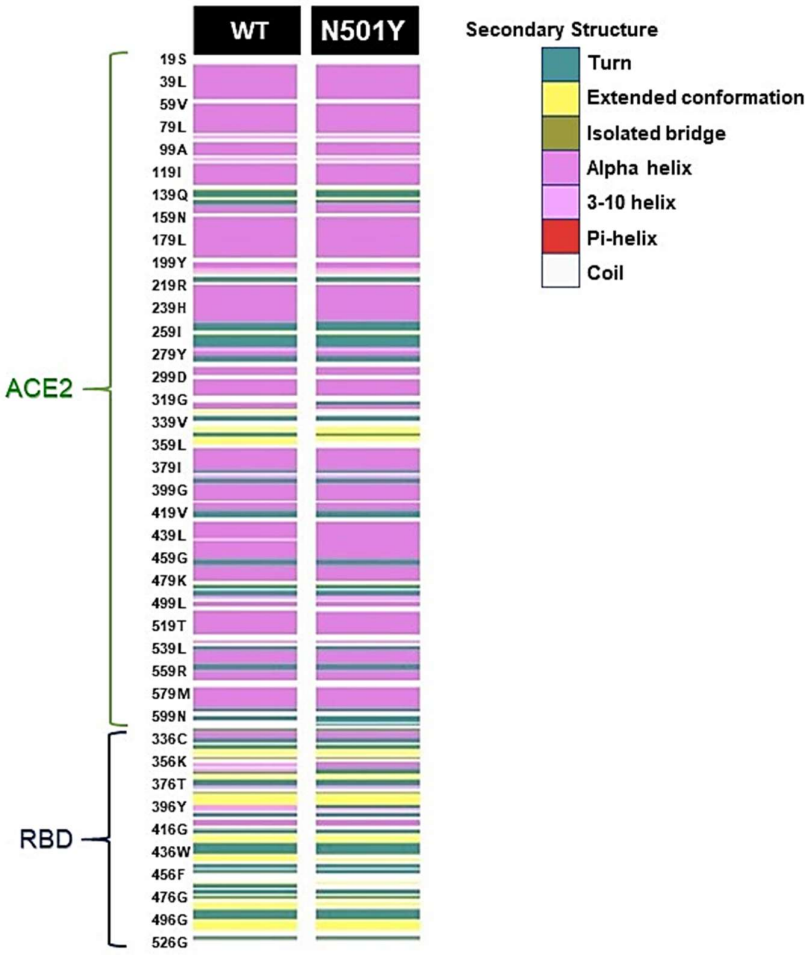

Figure 3 The secondary structure of WT and N501Y systems.

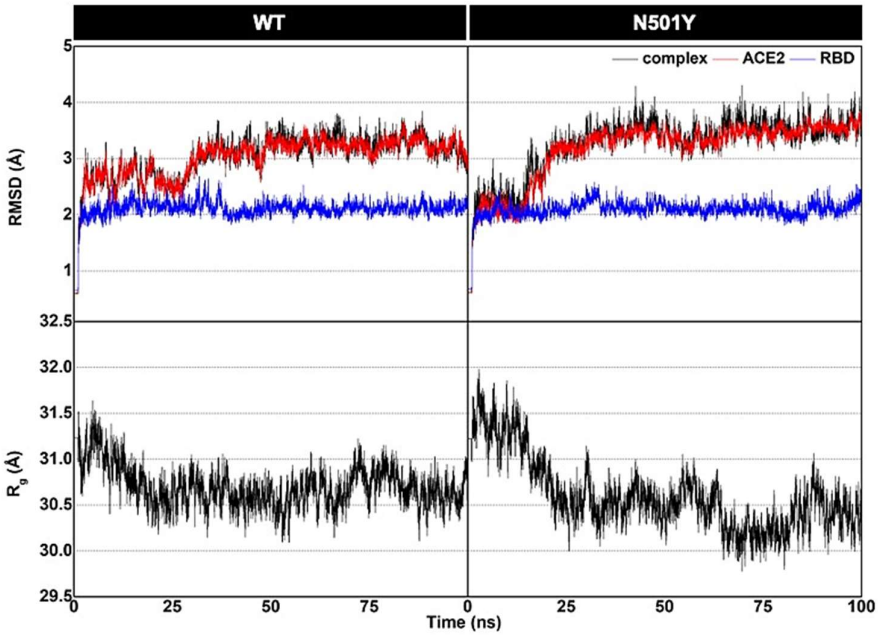

Figure 4 (Top) RMSD plots of all atoms of complex (black), ACE2 (red), and RBD (blue). (Bottom) R_g plots of RBD/ACE2 complexes.

3.3 Binding affinity between WT/N501Y-RBD and ACE2

To estimate the susceptibility of WT/N501Y-RBD to ACE2, MM/GBSA, MM/PBSA, and SIE binding free energy calculations were performed; the results are presented in Tables 1 and 2. The binding free energy values of the N501Y system ($\Delta G_{\text{bind}}^{\text{MM/PBSA}}$ = -63.24 ± 0.70, $\Delta G_{\text{bind}}^{\text{MM/GBSA}}$ = -44.42 ± 0.51, and $\Delta G_{\text{bind}}^{\text{SIE}}$ = -13.7 ± 0.07 kcal/mol) were found to be lower than those generated for the WT system (-49.43 ± 0.74, -37.16 ± 0.61, and -12.87 ± 0.07 kcal/mol, respectively), indicating that the N501Y mutation in the RBD of the SARS-CoV-2 S protein strengthens its binding to the human ACE2 receptor. The MM/GB(PB)SA results show that the N501Y mutation could increase vdW and electrostatic interactions in protein–protein binding compared to the WT model. In comparison, the SIE method suggests the enhancement of only vdW interactions due to the N501Y mutation.

Table 1 MM/PBSA and MM/GBSA binding free energies, $\Delta G_{\text{bind}}^{\text{MM/PBSA}}$ and $\Delta G_{\text{bind}}^{\text{MM/GBSA}}$ (kcal/mol), of WT- and N501Y-RBD in complex with the ACE2 receptor

	WT		N501Y	
	MM/PBSA	MM/GBSA	MM/PBSA	MM/GBSA
ΔE_{vdW}	-91.86 ± 0.68		-97.33 ± 0.58	
ΔE_{ele}	-582.43 ± 2.69		-587.94 ± 3.27	
ΔE_{MM}	-674.28 ± 2.90		-685.27 ± 3.29	
ΔG_{sol}	624.85 ± 2.65	637.12 ± 2.56	622.03 ± 3.24	640.85 ± 3.21
ΔG_{bind}	-49.43 ± 0.74	-37.16 ± 0.61	-63.24 ± 0.70	-44.42 ± 0.51

Table 2 SIE binding free energy, $\Delta G_{\text{bind}}^{\text{SIE}}$ (kcal/mol), of WT- and N501Y-RBD in complex with the ACE2 receptor

	WT	N501Y
ΔE_{vdW}	-91.55 ± 0.58	-97.33 ± 0.58
ΔE_c	-282.11 ± 1.30	-261.4 ± 1.45
ΔG^R	295.2 ± 1.22	272.34 ± 1.34
$\gamma \Delta MSA$	-16.77 ± 0.08	-16.8 ± 0.07
$\Delta G_{\text{bind}}^{\text{SIE}}$	-12.87 ± 0.07	-13.7 ± 0.07

3.4 The intermolecular hydrogen bonds between WT/N501Y-RBD and ACE2

The %H-bond was analysed to characterise the intermolecular interactions of the WT- and N501Y-RBD/ACE2 systems, as shown in Figures 5A and 5B, respectively. The results were considered at a > 40% occupation between H-bond donors and acceptors. The findings indicate that residue 501 presents a stronger H-bond in the N501Y-RBD/ACE2 system compared to the WT-RBD/ACE2 model. The substitution of asparagine with tyrosine in residue 501 leads to an increase in its %H-bond from 20.50% (interacting with Y41) to 41.27% (interacting with D38). Moreover, the N501Y mutation in the RBD enhances the formation of H-bonds with the ACE2 residues S19, D38, D355, and A386 (S19@OG…A475@O, D38@OD2…N/Y501@OH, D355@OD2…T500@OG1, and A386@O…Y505@OH, respectively). The increasing %H-bond occupation in the N501Y system indicates the increasing strength of the H-bond at the interface between the RBD and ACE2. The increasing H-bond strength decreases the distance between the donor and acceptor atoms of the amino acids in the binding site. Thus, the N501Y mutation in the RBD can promote the binding affinity between the RBD of the SARS-CoV-2 S protein and human ACE2 via increased %H-bonds and compactness.

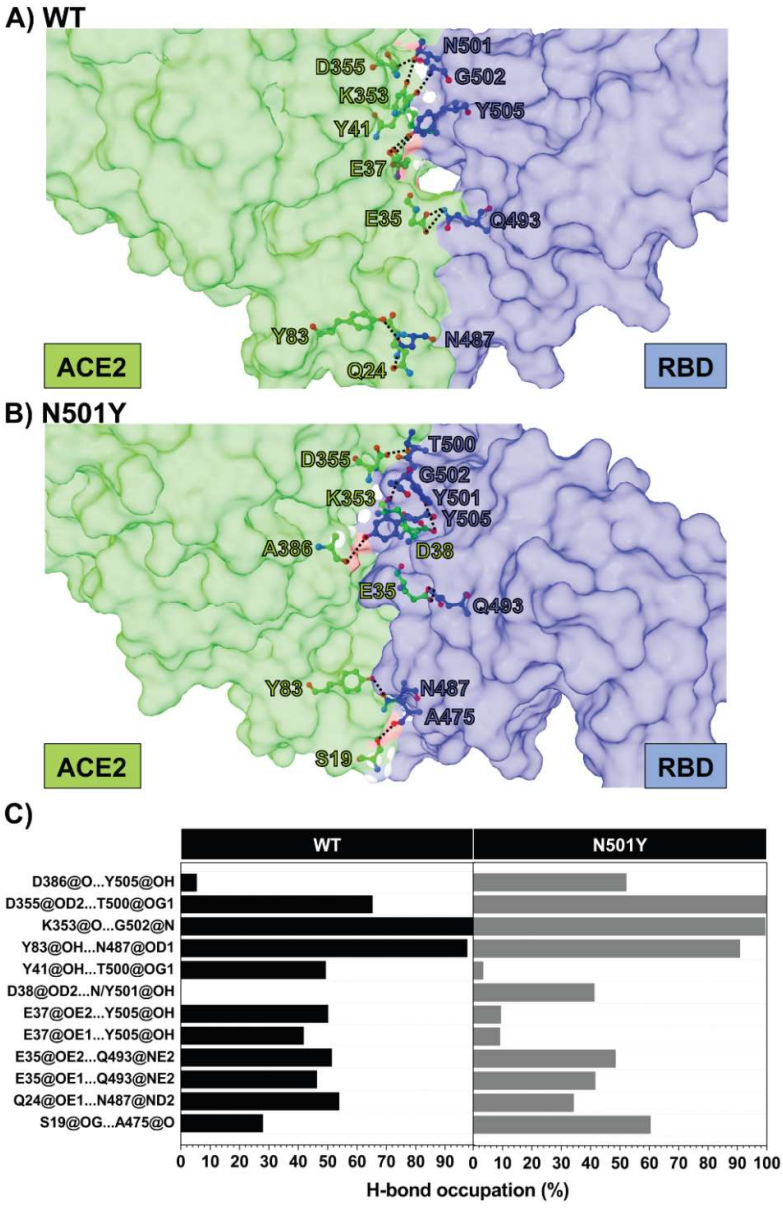

Figure 5 Intermolecular hydrogen bond interactions of RBD/ACE2 in the (A) WT- and (B) N501Y-RBD/ACE2 complexes, calculated from the trajectories from 70 to 100 ns; and (C) the percentage of H-bond occupation per residue.

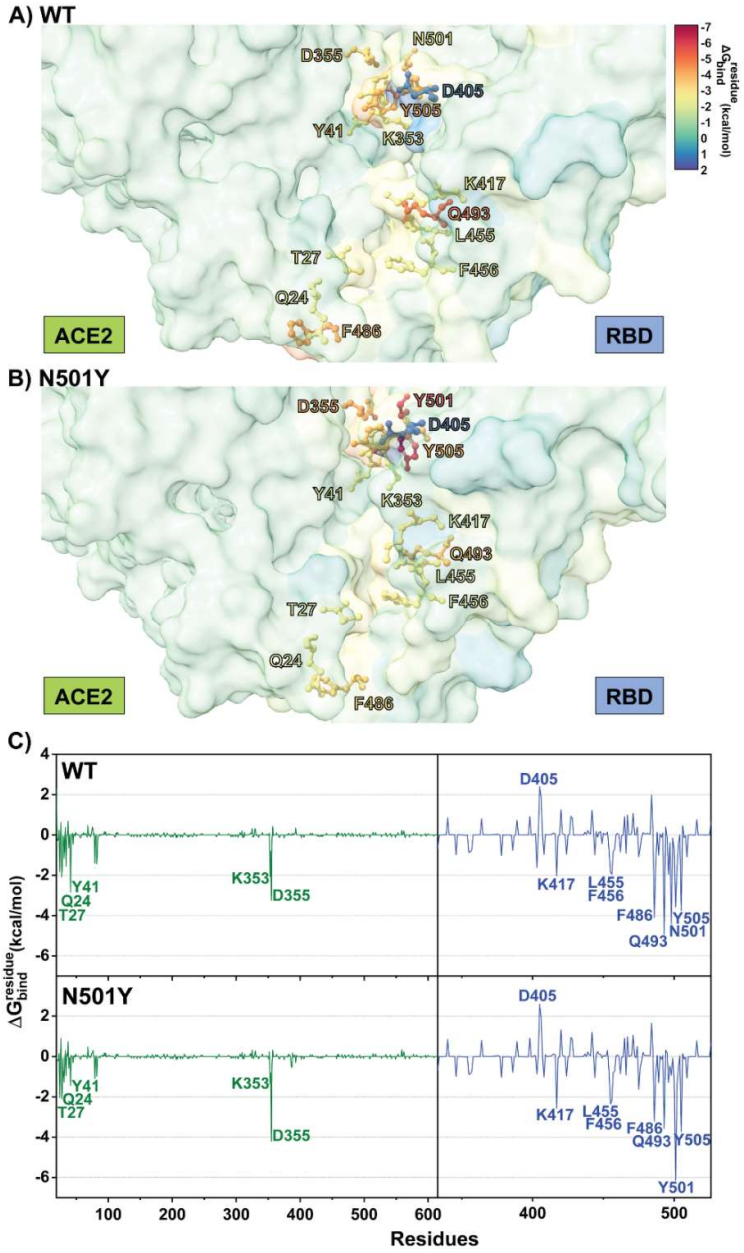

Figure 6 (A) Residues that have contribution energies ≤ -2.00 or ≥ 2.00 kcal/mol. $\Delta G_{\text{bind}}^{residue}$ between the RBD and ACE2 in the (B) WT-RBD/ACE2 and (C) N501Y-RBD/ACE2 systems, calculated from the trajectories between 70 and 100 ns of the simulation time.

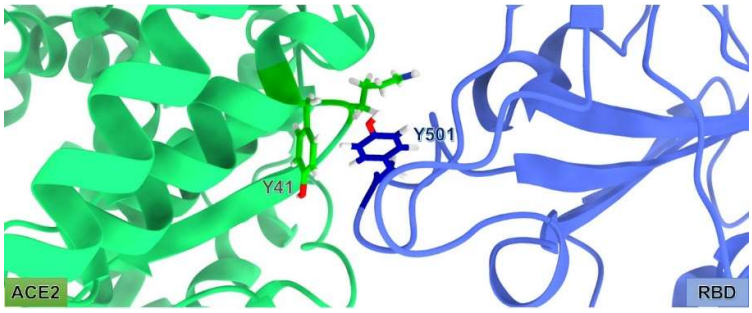

Figure 7 The final MD snapshot of the N501Y system showing interaction between Y41 and Y501.

3.5 Key binding residues of WT- and N501Y-RBD/ACE2 complexes

In this section, the MM/GBSA method was applied to investigate the key binding residues between the RBD and ACE2. The $\Delta G_{\text{bind}}^{residue}$ value was used to estimate the hot-spot residues of the RBD and ACE2 (Figure 6). In this study, the residues exhibiting energy stabilisation and destabilisation were taken at energies ≤ -2 and ≥ 2 kcal/mol, respectively. We identified ten (Q24, T27, D355, K417, L455, F456, F486, Q493, Y501, and Y505) and nine (T27, Y41, K353, D355, K417, F486, Q493, N501, and Y505) stabilising residues of the RBD associated with the binding of ACE2 in the N501Y and WT systems, respectively. In contrast, the destabilising residue (D405) was pronounced in both models. The increased susceptibility of hot-spot residues of N501Y-RBD, including Q24, D355, K417, L455, F456, and notably Y501 ($\Delta G_{\text{bind}}^{residue}$ from -1.82, -3.25, -2.03, -1.85, -1.94, and -3.58 kcal/mol to -2.03, -4.20, -2.57, -2.35, -2.17, and -6.15 kcal/mol, respectively), results in promoting the formation of H-bonds (Figure 5), as mentioned earlier. The increasing $\Delta G_{\text{bind}}^{residue}$ in the N501Y system compared to the WT one, for residues such as Q24, D355, L455, and notably Y501, has also been reported by Jawad et al. [30]. However, some residues of ACE2 (Y41, K353, D405, F486, and Q493) exhibit lower susceptibility towards the binding of N501Y-RBD. In the N501Y system, D38 (-0.58 kcal/mol) formed a strong H-bond with Y501 (Figure 5). In addition, the T-sharp π–π interactions between ACE2 Y41 and RBD Y501 (-1.44 kcal/mol) were also found in the N501Y system (Figure 7). This result indicates that the N501Y mutation could enhance the binding affinity compared to the WT-RBD system via strong H-bonds, π–π interactions, and vdW interactions. The ACE2-RBD interactions between Y41 and Y501, as well as that between K353 and Y501, correspond to the cryo-EM structure of the N501Y spike protein ectodomain bound to ACE2, showing that Y501 in the spike protein interacts with Y41 (π–π interactions) and K353 of ACE2 [15]. In addition, the binding affinity results are supported by those of the biolayer interferometry (BLI) technique. Furthermore, the Y501 can change its interactions within the binding site, while the secondary structure of the RBD and ACE2 (Figure 3) is similar to that of the WT system.

The RBD residue 501 interacting with the ACE2 receptor was studied and compared between the WT and N501Y systems using residue interaction network analysis with the RING 3.0 program. Figure 8 shows that Y501 can likely form H-bonds with D38, while the interaction with Y41 changes from H-bonding in the WT system to π–π stacking in the N501Y system. However, no H-bond with K353 was detected, resulting in a decreased K353 contribution to protein–protein binding, as depicted in Figure 6C.

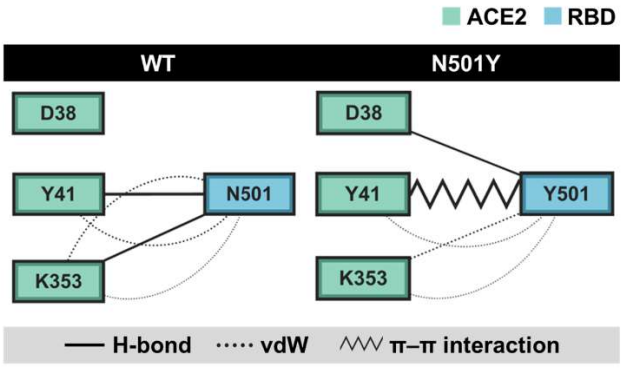

Figure 8 Residue interaction network between residue 501 in the RBD and its neighbouring ACE2 residues in the WT and N501Y systems. Only residue–residue interactions ≥ 40% are presented.

4. Conclusions

In this work, we investigated the dynamics of WT/N501Y-RBD interacting with ACE2 and their susceptibility using MD simulations and binding affinity calculations based on the MM/GBSA, MM/PBSA, and SIE methods. Our analysis showed that the susceptibility of the RBD to ACE2 in the N501Y-RBD/ACE2 system is higher than that in the WT-RBD/ACE2 system. Furthermore, the binding energy of the N501Y system was found to be more robust than that of the WT system. Residue interaction network analysis revealed that the formation of intermolecular interactions between the N501Y mutation in the RBD and the ACE2 residues was driven by the formation of H-bond (Y501-D38), π–π (Y501-Y41), and vdW (Y501-K353) interactions. Furthermore, *(i)* the enhanced susceptibility of N501Y-RBD hot-spot residues, such as Q24, D355, K417, L455, F456, and notably Y501; and *(ii)* the N501Y mutation could decrease the number of destabilising residues and promote H-bond

formation. Altogether, the N501Y mutation can reduce the number of destabilising residues at the protein–protein interface and may increase the binding affinity between the RBD and ACE2 during the fusion process in human membranes.

5. Acknowledgements

This project was funded by the National Research Council of Thailand (NRCT, grant number N42A650231). The Second Century Fund (C2F), Chulalongkorn University is acknowledged for providing PhD scholarships to N.K. We thank the ASEAN European Academic University Network (ASEA-UNINET) and the Computational Chemistry Center of Excellence and the Vienna Scientific Cluster (VSC).

6. References

[1] Organization WH. World Health organization (WHO) [Internet]. 2020 [cited 2022 Sep 14]. Available from: https://www.who.int/emergencies/diseases/novel-coronavirus-2019.
[2] Huang C, Wang Y, Li X, Ren L, Zhao J, Hu Y, et al. Clinical features of patients infected with 2019 novel coronavirus in Wuhan, China. The Lancet. 2020;395(10223):497-506.
[3] Marra MA, Jones SJM, Astell CR, Holt RA, Brooks-Wilson A, Butterfield YSN, et al. The genome sequence of the SARS-associated coronavirus. Science. 2003;300(5624):1399-1404.
[4] Rota PA, Oberste MS, Monroe SS, Nix WA, Campagnoli R, Icenogle JP, et al. Characterization of a novel coronavirus associated with severe acute respiratory syndrome. Science. 2003;300(5624):1394-1399.
[5] Tortorici MA, Veesler D. Chapter Four - Structural insights into coronavirus entry. In: Rey FA, editor. Advances in Virus Research (Volume 105). Cambridge: Academic Press; 2019. p. 93-116.
[6] Jackwood M, Hilt D, Callison S, Lee CW, Plaza H, Wade E. Spike glycoprotein cleavage recognition site analysis of infectious bronchitis virus. Avian diseases. 2001;45:366-372.
[7] Xu H, Zhong L, Deng J, Peng J, Dan H, Zeng X, et al. High expression of ACE2 receptor of 2019-nCoV on the epithelial cells of oral mucosa. Int J Oral Sci. 2020;12(1):8.
[8] Zhang H, Kang Z, Gong H, Xu D, Wang J, Li Z, et al. The digestive system is a potential route of 2019-nCov infection: a bioinformatics analysis based on single-cell transcriptomes. bioRxiv: the preprint server for biology. https://doi.org/10.1101/2020.01.30.927806.
[9] Davies NG, Abbott S, Barnard RC, Jarvis CI, Kucharski AJ, Munday J, et al. Estimated transmissibility and severity of novel SARS-CoV-2 Variant of Concern 202012/01 in England. medRxiv: the preprint server for health sciences. doi: https://doi.org/10.1101/2020.12.24.20248822.
[10] Greaney AJ, Loes AN, Crawford KHD, Starr TN, Malone KD, Chu HY, et al. Comprehensive mapping of mutations in the SARS-CoV-2 receptor-binding domain that affect recognition by polyclonal human plasma antibodies. Cell Host Microbe. 2021;29(3):463-476.
[11] Xie X, Zou J, Fontes-Garfias CR, Xia H, Swanson KA, Cutler M, et al. Neutralization of N501Y mutant SARS-CoV-2 by BNT162b2 vaccine-elicited sera. bioRxiv: the preprint server for biology. doi: https://doi.org/10.1101/2021.01.07.425740.
[12] Zhu X, Mannar D, Srivastava SS, Berezuk AM, Demers J-P, Saville JW, et al. Cryo-electron microscopy structures of the N501Y SARS-CoV-2 spike protein in complex with ACE2 and 2 potent neutralizing antibodies. PLOS Biology. 2021;19(4):e3001237.
[13] Luan B, Wang H, Huynh T. Enhanced binding of the N501Y-mutated SARS-CoV-2 spike protein to the human ACE2 receptor: insights from molecular dynamics simulations. FEBS Letters. 2021;595(10):1454-1461.
[14] Verkhivker G, Agajanian S, Kassab R, Krishnan K. Computer simulations and network-based profiling of binding and allosteric interactions of SARS-CoV-2 spike variant complexes and the host receptor: Dissecting the mechanistic effects of the delta and omicron mutations. Int J Mol Sci. 2022;23(8):4376.
[15] Homeyer N, Gohlke H. Free energy calculations by the molecular mechanics poisson−boltzmann surface area method. Mol Inform. 2012;31(2):114-122.
[16] Sulea T, Cui Q, Purisima EO. Solvated Interaction Energy (SIE) for scoring protein–ligand binding affinities. 2. benchmark in the CSAR-2010 scoring exercise. J Chem Inf Model. 2011;51(9):2066-2081.
[17] Lan J, Ge J, Yu J, Shan S, Zhou H, Fan S, et al. Structure of the SARS-CoV-2 spike receptor-binding domain bound to the ACE2 receptor. Nature. 2020;581(7807):215-220.
[18] Case D, Betz R, Cerutti DS, Cheatham T, Darden T, Duke R, et al. Amber 2016. San Francisco: University of California; 2016.
[19] Olsson MH, Sondergaard CR, Rostkowski M, Jensen JH. PROPKA3: Consistent treatment of internal and surface residues in empirical pKa predictions. J Chem Theory Comput. 2011;7(2):525-537.

[20] Maier JA, Martinez C, Kasavajhala K, Wickstrom L, Hauser KE, Simmerling C. ff14SB: Improving the accuracy of protein side chain and backbone parameters from ff99SB. J Chem Theory Comput. 2015;11(8):3696-3713.
[21] Leontyev IV, Stuchebrukhov AA. Polarizable mean-field model of water for biological simulations with AMBER and CHARMM force fields. J Chem Theory Comput. 2012;8(9):3207-3216.
[22] Mahalapbutr P, Lee VS, Rungrotmongkol T. Binding hotspot and activation mechanism of maltitol and lactitol toward the human sweet taste receptor. J Agric Food Chem. 2020;68(30):7974-7983.
[23] Elber R, Ruymgaart AP, Hess B. SHAKE parallelization. Eur Phys J Spec Top. 2011;200(1):211-223.
[24] Darden TA, York DM, Pedersen LG. Particle mesh Ewald: An N·log(N) method for Ewald sums in large systems. J Chem Phys. 1993;98(12):10089-10092.
[25] Roe DR, Cheatham TE. PTRAJ and CPPTRAJ: Software for processing and analysis of molecular dynamics trajectory data. J Chem Theory Comput. 2013;9(7):3084-3095.
[26] Clementel D, Del Conte A, Monzon AM, Camagni Giorgia F, Minervini G, Piovesan D, et al. RING 3.0: fast generation of probabilistic residue interaction networks from structural ensembles. Nucleic Acids Res. 2022;50(W1):W651-W656.
[27] Shannon P, Markiel A, Ozier O, Baliga NS, Wang JT, Ramage D, et al. Cytoscape: A software environment for integrated models of biomolecular interaction networks. Genome Res. 2003;13(11):2498-2504.
[28] Ramachandran GN, Ramakrishnan C, Sasisekharan V. Stereochemistry of polypeptide chain configurations. J Mol Biol. 1963;7(1):95-99.
[29] Anderson RJ, Weng Z, Campbell RK, Jiang X. Main-chain conformational tendencies of amino acids. Proteins. 2005;60(4):679-689.
[30] Jawad B, Adhikari P, Podgornik R, Ching WY. Key interacting residues between RBD of SARS-CoV-2 and ACE2 receptor: combination of molecular dynamics simulation and density functional calculation. J Chem Inf Model. 2021;61(9):4425-41.